Paper 259

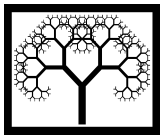

Proceedings of the Eleventh International Conference
on Computational Structures Technology,
B.H.V. Topping, (Editor),
Civil-Comp Press, Stirlingshire, Scotland

A Two-Scale Micromechanical Model for Closed-Cell Aluminium Foams

J. Němeček and V. Králík
Department of Mechanics, Faculty of Civil Engineering
Czech Technical University in Prague, Czech Republic

Abstract

This paper is focused on the assessment of effective elastic properties of closed-cell aluminium foams by means of a two-scale micromechanical model. The foam is characterized by a closed pore system with very thin pore walls (~0.1 mm) and large air pores (~2.9 mm). The lower level of the proposed model contains the inhomogeneous solid matter of the foam cell walls produced from aluminium melt with admixtures. Elastic parameters as well as volume fractions of microstructural material phases at this level are assessed with nanoindentation and effective properties computed using analytical and numerical homogenization schemes. The effective Young's modulus of the cell walls was found to be close to 70 GPa irrespective to the homogenization procedure used.

The upper level of the model contains homogenized cell wall properties and a significant volume fraction of air voids (91.4%). Since analytical schemes fail to predict effective properties of this highly porous structure, numerical homogenization based on simple two dimensional (2-D) finite element model is utilized. The model geometry is based on foam optical images and the beam structure is produced using Voronoi tessellation. Effective foam Young's modulus was found to be 1.1-1.2 GPa which is in relation with E~1.45 GPa obtained from uniaxial compression experiments. The stiffness underestimation in the 2-D model is caused likely by the lack of the real three-dimensional confinement that cannot be captured in this simplification or by insufficient RVE size. It leads to the necessity of model refinement and of further investigations in three dimensions.

Keywords: nanoindentation, aluminium foam, multi-scale model, homogenization, elastic properties.

1 Introduction

Foamed ceramics are characterized with high porosity, light weight, high mechanical strength, excellent impact energy absorption, high damping capacity,

good sound absorption capability, and many other attractive engineering properties. The usual source materials for the production of ceramic foam are melt metals like aluminium and aluminium alloys, titanium, silicon carbide, zirconia, etc. Metal foams are used in applications ranging from automotive and aerospace industries (e.g. bumpers, car body sills, motorcycle helmets, filters) to building industry (e.g. sound proofing panels). Our aim was to characterize and to model a foam called Alporas® produced by Shinko Wire Company, Ltd. [1], [2]. It is a highly porous aluminium foam that can reach the overall porosity more than 90%. Its microstructure is characterized with a hierarchical system of pores containing different cell morphologies (shape, size and distribution of cells) in dependence on the foam density and inhomogeneous material properties of the cell walls [3]. Typical cross section of the foam is shown in Figure 1.

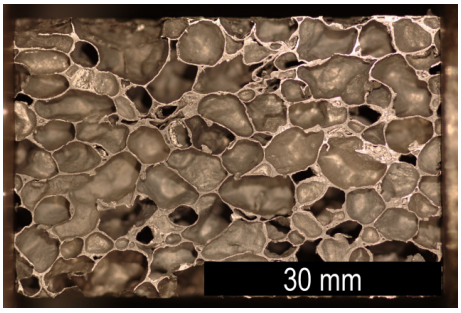

Figure 1: Cross section of the aluminium foam.

In our modeling, we focused on the prediction of the overall foam elastic properties and model validation against experimental results. For accessing the cell wall properties we employed statistical nanoindentation and deconvolution technique for the phase separation [4],[5]. Compared to traditional macroscopic techniques [6],[7],[8] nanoindentation can distinguish between individual inhomogeneous microstructural entities. The effective cell wall properties have been obtained through analytical and numerical up-scaling techniques [9]. Finally, simple 2-D finite element model for the upper composite scale has been proposed and results validated with experiments.

2 Material characterization

2.1 Material and sample preparation

The Alporas® foam is produced from melt alumina in which 1.5 wt.% of calcium is added to the aluminium molten at 680 °C [2]. Calcium serves as a thickening agent which increases viscosity and stabilizes the air bubbles. The alloy is poured into a casting mold and stirred with an admixture of 1.6 wt.% TiH_2 that is used as a blowing agent. Then, the foamed molten material is cooled down.

Firstly, a large panel of Alporas (160 × 100 × 60 mm) was polished and scanned with a high resolution scanner. Acquired images were segmented to binary ones and further used in image analyses. Then, a smaller Alporas block was cut into thin slices (~5 mm) and embedded into epoxy resin to fill the pores. The surface was mechanically grinded and polished to reach minimum surface roughness suitable for nanoindentation. Very low roughness $R_q \approx 10$ nm [10] was achieved on cell walls. The sample was investigated with electron microscopy (ESEM) and nanoindentation.

2.2 ESEM and element analysis

The ESEM analysis on cell walls revealed their inhomogeneous microstructural composition. It was found that a significant inhomogeneity of the microstrutural material phases exists on the level of tens of micrometers (Figure 2). Two distinct phases, that exhibit different color in back-scattered electron (BSE) images, can be distinguished. The chemical composition of the two phases was checked with EDX element analysis in ESEM. It was found that the majority of the volume (dark zone in Figure 1c, 2a) consists of aluminium (~67 wt.%), oxygen (~32 wt.%) and further trace elements (Mg, Ti, Fe, Co, Ni, Cu, Si <2 wt.%). Lighter zones in Figure 2 consist of Al (~60 wt.%), O (~30 wt.%), Ca (~5 wt.%), Ti (~5 wt.%) and other elements (<1 wt.%). As expected, the majority of the volume (dark zone) is composed of aluminum and aluminium oxide Al_2O_3 (further denoted as Al-rich area). Lighter zones contain significant amount of calcium and titanium (further denoted as Ca/Ti-rich area). The non-uniform distribution of these zones shows on inhomogeneous mixing of the admixtures that are added during the production process.

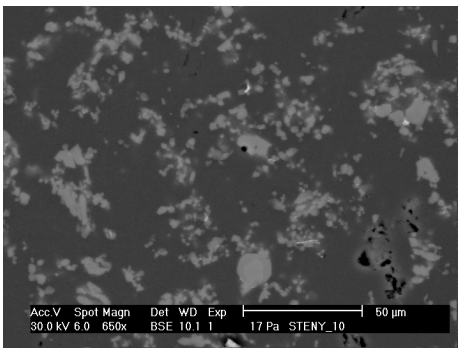

Figure 2: ESEM image of the cell wall (light=Ca/Ti-rich, dark=Al-rich area).

2.3 Porosity and image analysis

The overall porosity of the sample was assessed by weighing of a large Alporas panel (knowing the sample dimensions and solid mass density 2700 kg.m^{-3}). The porosity reached 91.4%. In other words, solid mass (cell walls) occupied only 8.6% of the total volume in the specimen.

The scanned sample was subjected to a careful image analysis which firstly included image segmentation to the binary image. Then, the distribution of cell wall thicknesses and the distribution of the pore sizes were studied by means of pore contour detection in the Matlab environment. At first, the contours were generated for every pore in the image and areal characteristics (centroid, area, second moment of inertia) were computed (Figure 3). The wall thicknesses were calculated as the minimum distance between the neighboring contours. The distribution of the thicknesses is shown in Figure 4. It can be seen in Figure 4 that a significant peak occurs around ~60 μm which can be understood as a characteristic cell wall thickness.

Then, equivalent ellipses were constructed from contour areal characteristics under the condition that they have the same area and the same principal second moment of inertia. Such assumption led to the evaluation of two main half axes (a_i and b_i) for each equivalent ellipse. In order to characterize the shape of pores, an equivalent ellipse shape factor was defined as the ratio

$$e_i = \frac{a_i}{b_i}. \qquad (1)$$

The distribution of the shape factor is depicted in Figure 5. It can be concluded that pores have typically a round shape with the shape factor lying mostly between 1 and 2. The peak with the highest occurrence in Figure 5 appears around e_i=1.15.

Due to the round shape of pores it makes sense to compute also an equivalent pore diameter using circular pore replacement. The distribution of equivalent circular pores is depicted in Figure 6. Wide distribution of pores with diameters 0-6 mm was found. The mean equivalent diameter was found to be 2.9±1.5 mm for the specific specimen.

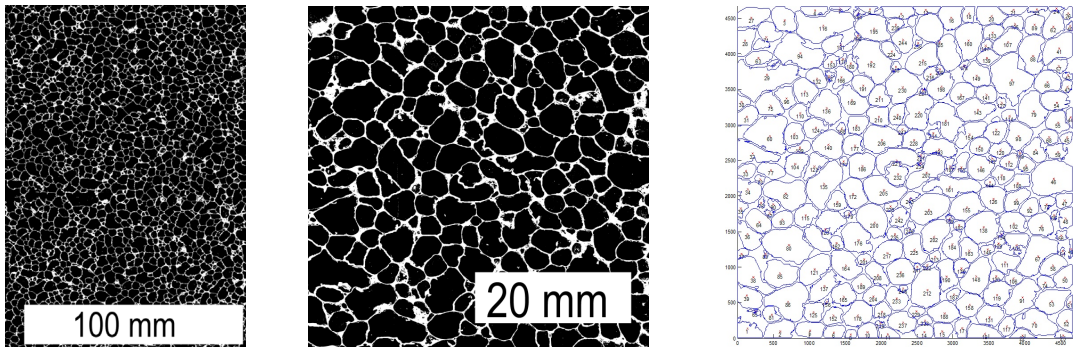

(a) (b) (c)

Figure 3: (a) Binary image of the polished foam panel. (b) Binary image of ~50×50 mm foam cut. (c) Cell contours in the cut.

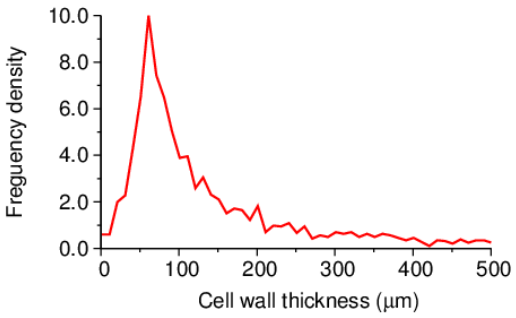

Figure 4: Distribution of cell wall thicknesses.

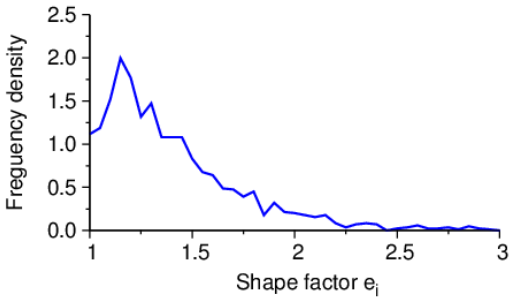

Figure 5: Distribution of equivalent ellipse shape factor.

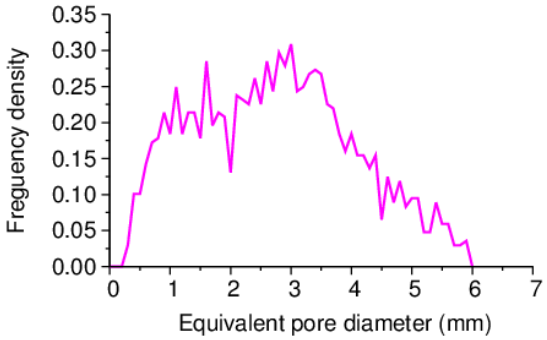

Figure 5: Distribution of equivalent circular pores.

2.4 Nanoindentation

Individual phase properties of cell walls were studied with nanoindentation. The tests were performed using Hysitron Tribolab system® at the Czech Technical University. Multiple locations on cell walls were tested and elastic properties evaluated for a large grid of indents (100×100 μm) representing the lower material scale. Statistical deconvolution was applied and Young's moduli and volume fraction of two microstructural phases extracted from frequency plots (Figure 6). In accordance with the ESEM analysis the two phases were denoted as Al-rich and Ca/Ti-rich zones. Experimental details and details on the deconvolution can be found e.g. in [5], [11]. Table 1 summarizes the results for the two phases in terms of mean elastic properties and volume fractions.

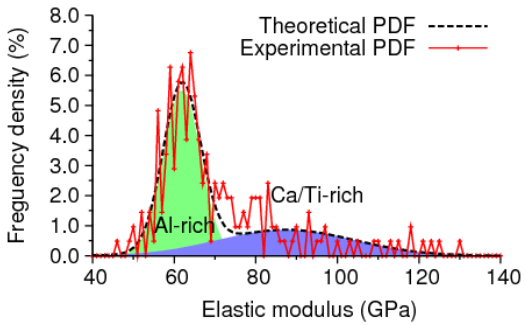

Figure 6: Probability density function of Young's modulus showing the two deconvoluted phases.

Phase	Mean (GPa)	St. dev. (GPa)	Volume fraction (-)
1 (Al-rich zone)	61.88	4.6	0.638
2 (Ca/Ti-rich zone)	87.40	16.7	0.362

Table 1: Young's moduli and volume fractions from nanoindentation.

3 Modeling

3.1 Definition of scales

The multiscale approach was utilized in this work and the material was described by two distinct levels - the cell wall level and the foam level. Each level, which is defined by a characteristic length, can be substituted by a macroscopically homogeneous representative volume element (RVE, [9]) which statistically represents the material level and serves for the evaluation of effective (homogenized) properties. The two levels of the proposed model with their microstructural inhomogeneities are as follows:

- **Level I** (the cell wall level) has a characteristic dimension defined by the mean midspan wall thickness L_I~60 μm. This level consists of prevailing aluminium matrix (Al-rich area) with embedded heterogeneities in the form of Ti/Ca-rich areas. Intrinsic elastic properties of the constituents were assessed by nanoindentation at this level. Individual indent size was prescribed to be considerably smaller (h≈100-300 nm) than a characteristic size of Ca/Ti inhomogeneities (~4 μm).
- **Level II** (the foam level) has a characteristic dimension of L_{II}~50 mm. At this level, large pores with an average equivalent diameter ~2.9 mm (assuming circular pores) are present in the volume of 91.4%. Cell walls are considered as homogeneous having the properties that come from the Level I homogenization.

3.2 Effective elastic properties of Level I

In this work, continuum micromechanics was applied to find effective elastic properties of the Level I RVE. Analytical homogenization methods are often based on classical Eshelby's solution [11] that uses an assumption of the uniform stress field in an ellipsoidal inclusion embedded in an infinite body. Effective elastic properties in RVE are then obtained through averaging over the local contributions. From the material point of view, composite materials are usually characterized by a prevailing matrix phase, which serves as a reference medium in homogenization methods, reinforced with geometrically distinguishable inclusions. For example, the Mori-Tanaka method [13] can be appropriate for these cases. Polycrystalline metals, in which no preference of matrix phase exists, are usually modeled with the self-consistent scheme [9] in which the reference medium refers back to the homogenized medium itself. Regardless the most suitable homogenization technique, which would be probably the Mori-Tanaka method in our case, we used multiple estimates assuming spherical inclusions. Namely, the Mori-Tanaka method, self-consistent scheme, Voigt and Reuss bounds (parallel or serial configuration of phases with perfect bonding). Results from nanoindentation have been used as input parameters to the methods. Negligible differences and very close bounds have been found for the specific case of Level I homogenization as summarized in Table 2. The result for Mori-Tanaka method is considered in further computations.

Scheme	Mori-Tanaka	Self-consist. Scheme	Voigt bound	Reuss bound
$E_{Level\ I}$ (GPa)	70.083	70.135	71.118	69.195

Table 2: Values of the Level I effective Young's modulus computed by different homogenization schemes.

In order to verify simple analytical schemes a numerical FFT-based method was applied. The method was proposed by Moulinec and Suquet [14] and is based on an integral (Lippmann–Schwinger type) equation:

$$\boldsymbol{\varepsilon}(\mathbf{x}) + \int_{\Omega} \Gamma^0(\mathbf{x}-\mathbf{y}) : (\mathrm{L}(\mathbf{y}) - \mathrm{L}^0) : \boldsymbol{\varepsilon}(\mathbf{y}) d\mathbf{y} = \mathbf{E} \qquad (2)$$

where $\boldsymbol{\varepsilon}(\mathbf{x})$ is the second order strain tensor, $\mathrm{L}(\mathbf{x})$ the fourth order tensor of elastic stiffness at individual locations $\mathbf{x}$ or $\mathbf{y}$, Γ^0 stands for the integral kernel which can be approximated by trigonometric polynomials in the Fourier space and $\mathbf{E}$ is a macroscopic strain tensor. After discretization, the solution leads to the assessment of a nonsymmetric linear system of equations which uses only the stiffness coefficients at discretization (grid) points. The system can be resolved e.g. by the conjugate gradient method as proposed in Zeman et.al. in [15]. Elastic constants

received from grid nanoindentation have been used as input parameters for this FFT homogenization with the assumption of plane strain conditions.

Resulting homogenized stiffness matrix is generally anizotropic. However, in our case the matrix was found to be very close to the isotropic stiffness matrix computed from the Mori-Tanaka Young's modulus in our case. The difference between the matrices in terms of the matrix error norm was found to be less than 4%. Therefore, it can be concluded that a very good agreement between the analytical and FFT-based numerical schemes was achieved.

3.3 Effective elastic properties of Level II

At this level, the cell walls are considered as a homogeneous phase having the properties that come from the Level I homogenization. The solid phase is very sparse in the sample volume due to its porosity (91.4% of air).

We firstly tried to estimate effective elastic properties with the same analytical schemes used at Level I. The result is summarized in Table 3. Voigt and Reuss bounds are quite distant in this case. Unfortunately, simple analytical schemes also fail to predict correctly the composite stiffness due to the extreme sample porosity. The Mori-Tanaka method approaches the arithmetic mean between the bounds, whereas the self-consistent scheme tends to reach the stiffness of the phase with higher occurrence (i.e. the air).

Scheme	Mori-Tanaka	Self-consist. Scheme	Voigt bound	Reuss bound
$E_{Level\ II}$ (GPa)	3.1510	0.0012	6.0200	0.0011

Table 3: Values of the Level II effective Young's modulus computed by different analytical homogenization schemes.

Most of analytical studies on the homogenization of foams are based on models with a regular periodic microstructure [16],[17]. Nevertheless, real foam microstructures are characterized with different sizes and shapes and sizes of pores rather than with periodic structures as shown in Section 2 of this paper. The solution can be to solve the problem of irregular microstructures by an analysis of a large representative volume element containing large enough number of pores. Such model can be solved in two or three dimensions.

Therefore, more appropriate two-dimensional microstructure based FEM model was proposed. The model geometry was generated from high resolution optical image of polished foam cross-section (Figure 7a) converted to binary one. Square domain with 106×106 mm size (i.e. being much larger than average pore size ~2.9 mm) was extracted from the image. At this domain, pore centroids were detected, Delaunay triangulation applied and Voronoi cells created. Then, an equivalent 2D-beam structure was generated from Voronoi cell boundaries (Figure 7b). Based on several numerical studies, it was found that the distribution of cross sectional areas and bending stiffness of individual beams do not play a

significant role in the evaluation of the homogenized properties. Therefore, as an approximate but sufficient estimate, uniform cross-sectional area was prescribed to all beams (taken from porosity measurement as ~8.6% of the total area).

In the analysis, macroscopic strain $\mathbf{E}$ is prescribed to the RVE and microscopic strains and stresses are solved. Volumetric averaging of microscopic stresses leads to the assessment of an average macroscopic stress and finally estimation of effective stiffness parameters. The key issue of the computation is the size of RVE and application of boundary conditions around the domain. Since the RVE size is always smaller than an infinite body, any constraints can strongly influence the results. Application of the kinematic boundary conditions leads to the overestimation of effective stiffness and it can give an upper bound, whereas the static boundary conditions give a lower bound [18]. The best solution is usually provided by applying periodic boundary conditions to RVE which are, however, difficult to implement into commercial codes.

Nevertheless, the influence of the boundary conditions on microscopic strains and stresses in the domain decrease in distant points from the boundary. The size of our domain (106×106 mm) allowed us to solve the problem with kinematic boundary conditions. For homogenization, considerably smaller region (20×20 mm or 30×30 mm) was used. Microscopic strains and stresses were computed inside this smaller area which was assumed to be still sufficiently large to describe the material inhomogeneities and to serve as material RVE.

Constrains were applied on all domain sides. Free beams located around the boundary and not connected to any cell were deleted and supports put on the nodes located on the closest cell. Such arrangement of beams and supports prevented the structure from unreasonably large deformations of these free boundary beams. The whole domain (106×106 mm) was subjected to homogeneous macroscopic strain in one axial direction ($\mathbf{E}=\{1,0,0\}^T$) by imposing prescribed displacement to one domain side (Figure 7b). The test was performed using Ansys software and microscopic strains and stresses solved in the domain. Strains and stresses (structural forces for the case of beams, respectively) inside the smaller area (20×20 mm or 30×30 mm) were averaged and used for computation of the homogenized stiffness matrix (one column in the matrix, respectively). Assuming material isotropy, the (1,1) member at the material stiffness matrix is given by:

$$L_{11} = E\frac{(1-\nu)}{(1+\nu)(1-2\nu)} \tag{3}$$

in which E is the Young's modulus and ν Poisson's ratio, respectively. Since the Poisson's ratio of the whole foam is close to zero (as confirmed by experimental measurements) the L_{11} member coincides with the Young's modulus E. For the tension test in x-direction (Figure 7b), the homogenized Young's modulus was found to be $E_{Level\ II}$= 1.11 GPa for RVE size 20×20 mm and $E_{Level\ II}$=1.21 GPa for RVE size 30×30 mm. The obtained 9% difference illustrates the dependence of the results on RVE size which was also observed experimentally. Experimental investigations of

the dependence of sample size on apparent elastic modulus and strength were conducted e.g. by Ashby et al. [19]. They found, the modulus and strength become independent of size when the sample dimensions exceeded about seven cell diameters. For our typical cell size (2.9 mm) we get 6.9 and 10.3 cell diameters for our 20 and 30 mm wide RVEs. So, such condition is satisfied for both RVEs. On the other hand, the RVE size should not exceed roughly 1/3 of the whole domain size not to be influenced by boundary conditions which implies maximum RVE width about 35 mm for our 106 mm wide domain. However, deeper investigation on the RVE size with respect to the effect of boundary conditions would lead to refinement of the estimate.

The resulting homogenized Young's modulus is comparable with the range of experimental values (0.4−1 GPa) reported for Alporas® e.g. by Ashby et. al. [19]. It is lower than results obtained from our experimental measurements (uniaxial compression test on 30×30×60 mm Alporas blocks) that indicate E≈1.45 GPa. The lower stiffness obtained from two-dimensional model can be explained by the lack of additional confinement appearing in the three-dimensional case. Therefore, the results of the simplified 2-D model have to be treated as a first estimate of the Level II material properties which need to be refined. The influence of the RVE size can also play a role.

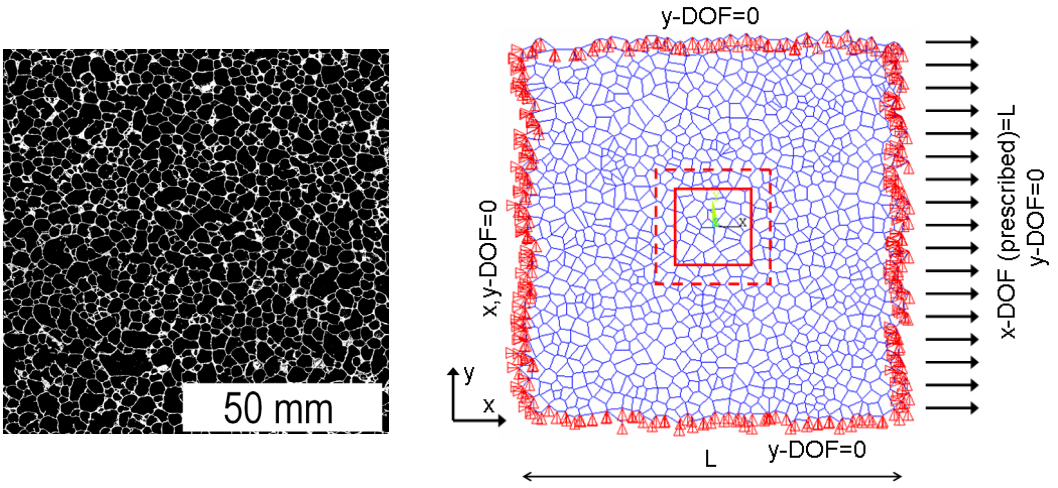

(a) (b)

Figure 7: (a) Binary image of the foam (106×106 mm). (b) 2-D beam model with boundary constraints (red square indicates area from which homogenized properties have been obtained; solid line=20×20 mm, dashed line=30×30 mm).

4 Conclusions

In this paper, two-scale microstructure based model of closed-cell aluminium foam was proposed for the assessment of effective elastic properties. The first level characterized by thin cell walls (RVE~60 μm) was successfully homogenized with

several analytical continuum mechanics schemes. Two different material phases (Al-rich and Ca/Ti-rich) were detected at this lower scale by statistical grid nanoindentation. Effective Young's modulus $E_{Level\ I} \approx 70$ GPa was received regardless the used scheme. The value was also justified by numerical FFT-based homogenization with a very good agreement (error less than 4%).

The upper foam level containing homogenized walls and large air pores was assumed for homogenization of the second level. Analytical tools applied on the first level were used without success. Very poor estimates were given by the Mori-Tanaka or self-consistent due to extremely high air content in the foam. To better describe the real foam microstructure, a two-dimensional FEM model was proposed for the numerical homogenization at the second level. The model geometry was generated from large optical scan of polished foam cross section converted to binary image. Delaunay triangulation and Voronoi tessellation have been applied and equivalent beam structure generated. It was discussed that using different boundary conditions have a strong impact on the resulting computed effective properties. Using of periodic boundary conditions was found to be algorithmically difficult to implement into commercial code (Ansys). Therefore kinematic constrains in the form of boundary supports were used on a large domain (106×106 mm) whereas microscopic strains and stresses were homogenized in much smaller area (20×20 mm or 30×30 mm) far from the boundary. Such model was found to realistically describe macroscopic elastic properties. Nevertheless, two-dimensional approximation underestimated the overall stiffness by 20-30% compared to experimental values. It is likely due to the inability to capture additional confinement coming from three-dimensional material microstructure or due to the insufficient RVE size. Further development of the numerical model and generation of the model geometry from micro-CT data (i.e. extension to 3-D) are planned as the future developments.

Acknowledgements

The financial support of the Grant Agency of the Czech Republic (GAČR P105/02/0824) and the Grant Agency of the Czech Technical University in Prague (SGS12/116/OHK1/2T/11) is gratefully acknowledged.

References

[1] J. Banhart, "Manufacture, characterisation and application of cellular metals and metal foams", Progress in Materials Science 46: 559-632, 2001.

[2] T. Miyoshi, M. Itoh, S. Akiyama, A. Kitahara, "Aluminium foam "ALPORAS": The production process, properties and application" Materials Research Society Symp. Proc. 521, 1998.

[3] M.A. Hasan, A. Kim, H.-J. Lee, "Measuring the cell wall mechanical properties of Al-alloy foams using the nanoindentation method", Composite Structures 83: 180-188, 2008.

[4] G. Constantinides, F.R. Chandran, F.-J. Ulm, K.V. Vliet, "Grid indentation analysis of composite microstructure and mechanics: Principles and validation", Materials Science and Engineering: A, 430 (1-2):189-202, 2006.
[5] J. Němeček, V. Šmilauer, L. Kopecký, "Nanoindentation characteristics of alkali-activated aluminosilicate materials", Cement and Concrete Composites 33 (2): 163-170, 2011.
[6] D.P. Papadopoulos, I.C. Konstantinidis, N. Papanastasiou, S. Skolianos, H. Lefakis, D.N. Tsipas, "Mechanical properties of Al metal foams", Materials Letters 58 (21): 2574-2578, 2004.
[7] I. Jeon, "Cell wall mechanical properties of closed-cell Al foam", Mechanics of Materials, 41 (1): 60-73, 2009.
[8] Y. Sugimura, J. Meyer, M.Y. He, H. Bart-Smith, J. Grenstedt, A.G. Evans, "On the mechanical performance of closed cell Al alloy foams", Acta Mater. 45: 5245–5259, 1997.
[9] A. Zaoui, "Continuum Micromechanics: Survey", Journal of Engineering Mechanics 128, 2002.
[10] ISO 4287-1997, "Geometrical Product Specifications (GPS) - Surface texture: Profile method - Terms, definitions and surface texture parameters".
[11] J. Nemecek, V. Králík, J. Vondrejc, J. Nemecková, "Identification of Micromechanical Properties on Metal Foams using Nanoindentation", in B.H.V. Topping, Y. Tsompanakis, (Editors), "Proceedings of the Thirteenth International Conference on Civil, Structural and Environmental Engineering Computing", Civil-Comp Press, Stirlingshire, UK, Paper 125, 2011. doi:10.4203/ccp.96.125
[12] J.D. Eshelby, "The determination of the elastic field of an ellipsoidal inclusion and related problem", Proc. Roy. Soc. London A 241: 376–396, 1957.
[13] T. Mori, K. Tanaka, "Average stress in matrix and average elastic energy of materials with misfitting inclusions", Acta Metallurgica 21 (5): 571-574, 1973.
[14] H. Moulinec, P. Suquet, "A fast numerical method for computing the linear and nonlinear mechanical properties of composites", Comptes rendus de l'Académie des sciences. Série II, Mécanique, physique, chimie, astronomie, 318(11): 1417-1423, 1994.
[15] J. Zeman, J. Vondřejc, J. Novák, I. Marek, "Accelerating a FFT-based solver for numerical homogenization of periodic media by conjugate gradients", Journal of Computational Physics, 229(21): 8065-8071, 2010.
[16] L.J. Gibson, M.F. Ashby, "Cellular Solids: Structure and Properties", Cambridge University Press, 1999.
[17] J. Hohe, W. Becker, "A probabilistic approach to the numerical homogenization of irregular solid foams in the finite strain regime", International Journal of Solids and Structures 42, 3549–3569, 2005.
[18] V. Šmilauer, Z. Bittnar, "Microstructure-based micromechanical prediction of elastic properties in hydrating cement paste", Cement and Concrete Research 36, pp.1708–1718, 2006.
[19] M.F. Ashby, A.G. Evans, N.A. Fleck, L.J. Gibson, J.W. Hutchinson, H.N.G. Wadley, "Metal Foams: A Design Guide", Butterworth-Heinemann, 2000.